https://jksus.org

Journal of King Saud University – Science

2025 37 (2) 5502024

Research Article

WeldiNet: An improved design of a Rigdelet neural network for welding defect detection based on an enhanced pufferfish optimization algorithm

Tianmeng Ren[a,*]

[a]Department of Chengdu Aeronautic Polytechnic, Chengdu Aeronautic Polytechnic, Chengdu, 610100, Sichuan, China

ARTICLE INFO

Keywords:
Defect detection
Enhanced pufferfish optimization algorithm
Rigdelet neural network
WeldiNet
Welding

ABSTRACT

The presence of possible defects in welding can lead to many risks, so identifying these defects is very important. Therefore, in recent years, the automatic detection of these defects using artificial intelligence techniques has also received a lot of attention. The present study presents an enhanced approach for welding defect detection based on a hybrid deep learning technique. The method uses Ridgelet Neural Network (RNN) as a non-destructive detection technique for the detection of welding defects. The study uses an enhanced variant of the Pufferfish Optimization Algorithm (EPOA) for optimizing the parameters of the RNN. The proposed approach is validated using a standard dataset, namely GDXray, and its results are compared with some state-of-the-art methods to show the method's superiority. The findings indicate that the proposed RNN/EPOA model can effectively identify various welding defects.

1. Introduction

Welding is an important element in the production and manufacture of metal materials and is used in various types of industries. Among the main applications of welding, we can mention the construction of large metal structures such as bridges, buildings, and means of transportation, and forging, which must have high welding quality (Vasan *et al.*, 2024). Also, in the automotive industry, welding is very important in the production and repair of automotive parts. In addition, welding is the main part of the production process in the marine industry, aircraft manufacturing, and the production of electrical and electronic devices. Welding defects cost a lot of money (Mustafa *et al.*, 2024).

Non-destructive tests are one of the most important technical tools for inspecting various welded parts. In the welding process, it is very important to identify welding defects in the performance of parts and structures, and techniques such as radiography, which can determine their information without destroying or changing parts, are more important (Block *et al.*, 2024). Due to the X-ray diffraction from the material and other electronic effects of the imaging system, usually the recorded images are accompanied by the effects, and in some cases, they do not have the required quality, or the image is distorted and making it difficult to detect defects (Cui *et al.*, 2024).

Welding radiography is one of the types of NDT to find internal defects and discontinuities in small and large metal structures. Due to the high cost of this welding inspection method, the radiation welder or welding test expert must have the necessary knowledge to interpret the radiographic film and find all types of defects in it, so as not to waste money and time (Li *et al.*, 2024). Image processing methods are used to solve these problems.

Due to the rapid development of machine vision technology, research on welding image defects using X-ray has been of interest to researchers. Here, welding joints, which are the main weaknesses in welding, and welding methods are examined using defect detection algorithms. In order to improve the efficiency of X-ray welding image detection, deep learning networks and double exposure algorithms are also used to identify welding defects, which improves the accuracy and speed of the inspection process (Zhang *et al.*, 2024).

Therefore, different algorithms based on image processing, machine vision, deep learning, and other relevant observations were used to identify and classify welding defects from radiographic images.

For example, Madhav *et al.* (Madhav *et al.*, 2023) aimed to assess and improve the welding operations' accuracy by conducting and using Deep Convolutional Neural Networks (DCNN). Incomplete or missing weld procedures can be recognized in an accurate manner by the suggested DCNN. There were the number of 10000 Not-OK and OK pictures in the training set that assessed the DCNN. After that, the network was made, assessed, and optimized to identify flaws in welding. The output of the model was examined, and the findings represented that the DCNN could forecast the flaws with good accuracy. The accuracy could be enhanced by 99.01% by the use of data augmentation once the training procedure was accomplished with 9,600 pictures.

Block *et al.* (Block *et al.*, 2024) represented LoHi-WELD, which was a public and original dataset to overcome the issues relevant to weld flaw classification and identification that were of 4 diverse types, including stains, discontinuities, deposits, and pores. There were the number 3022 actual weld bead pictures that were annotated in a manual manner for visual examination. They consisted of images with high- and low-resolution, which were obtained from a Metal Active Gas robotic welding procedure. A diversity of a baseline deep framework for the suggested database was explored on the basis of the YOLOv7 network; moreover, several case investigations were discussed. The mean average precision (mAP) value of a fine-grained flaw categorization was 0.69,

***Corresponding author**
E-mail address: rentianmeng888@126.com (T. Ren)

Received: 26 December, 2024 **Accepted:** 06 May, 2025 **Published:** 31 May 2025

DOI: 10.25259/JKSUS_550_2024

and the value of a coarse categorization was 0.77, which were achieved by a lightweight framework.

Palma-Ramírez *et al.* (Palma-Ramírez *et al.*, 2024) presented a kind of CNN on the basis of ResNet50 to categorize 4 diverse kinds of weld flaws within radiographic images, including no defect, non-penetration, pore, and crack. Regularization, data, augmentation, and stratified cross-validation were employed to avoid over-fitting and enhance generalization. The model was examined using three diverse databases, including a private dataset of low image quality, GDXray, and RIAWELC, which in turn, accomplished accuracy values of 75.83%, 90.25%, and 98.75%.

Yadav *et al.* (Yadav *et al.*, 2024) employed a CNN-SVM hybrid model and assessed it on the basis of several evaluation metrics with the purpose of welding flaw categorization. There were several flaw categories, including Slag Inclusion, Undercut, Porosity, Cracks, and Ideal Weld. For these categories, the suggested model had the values of more than 96% for F1-score, recall, and precision. The suggested model could classify the defects with an accuracy value of 96.92 using a database with 4880 images. The results demonstrated that the model could perform well and was superior to other models existing in the study. However, there might be some problems in the robustness and reliability of the current model.

Vasan *et al.* (Vasan *et al.*, 2024) suggested a deep learning method on the basis of the ensemble for detecting and monitoring immersed weld flaws in adjacent regions and weld beads throughout Non-Destructive Testing (NDT). The approach made use of an open-source dataset to classify immersed arc weld classes into three categories of defects, including lack of penetration, cracks, no defects, and porosity. To improve the investigation of images, preprocessing and feature extraction techniques were implemented in frequency and spatial domains while utilizing segmentation methods, such as the Grey Level Co-occurrence Matrix (GLCM), Grey Level Difference Method (GLDM), texture analysis, Fast Fourier Transform (FFT), and Discrete Wavelet Transform (DWT). Once the preparation of images has been conducted, the preprocessed data undergoes testing and training in the suggested deep learning model on the basis of the ensemble. The efficacy of the model was generally evaluated by the use of several evaluation metrics. Moreover, it is worth noting that the model could accomplish an accuracy value of 93.12% for the categorization and detection of faults in welding.

Ridgelet neural networks (RNNs) are one of the deep learning techniques that can be used as an efficient tool for image-based defect detection. However, using the conventional methods for selecting the RNN structure is not so promising. Using metaheuristics in this task is a better way to resolve this issue.

The Pufferfish Optimization Algorithm (POA) is a newly introduced metaheuristic algorithm with lucky solutions for complicated optimization problems. In addition, based on the free lunch theorem, the original POA may not be so effective in optimizing the structure of the RNN. So, providing an enhanced version of this algorithm can be useful for welding defect detection.

The present study provides a new framework for detecting welding defects through the use of an RNN that is optimized by an enhanced variant of the POA. The proposed methodology will be tested on a dataset comprising welding images that exhibit a range of defects.

2. Data source benchmark

The present study uses the “GDXray” benchmark dataset for validating the proposed model. The GDXray consists of 19,407 x-ray images for weld defect detection, which is collected by Brewster Angle Microscopy (BAM) (Carrasco Zambrano 2023). The dataset is divided into five categories: welds, castings, natural entities, and luggage, each containing multiple series of images. For this study, we focus on the “welds” category, which comprises 88 images organized into three series: “W0001”, “W0002”, and “W0003”.

Series W0001 and W0002 contain 10 x-ray images each, while series W0003 consists of 68 digitized radiographs images (Mery *et al.*, 2015) (Table 1). These images represent various types of weld defects, including porosity, cracks, and lack of fusion, making them suitable for evaluating the performance of the proposed weld defect detection method.

Fig. 1. Some samples of the GDXray dataset for welding.

Fig. 1 shows some samples of the GDXray dataset.

The GDXray dataset can be considered a trustworthy and standardized reference for assessing the effectiveness of the proposed method, removing the necessity for costly X-ray machinery and guaranteeing the consistency of the results.

3. Methodology

Fig. 2 shows the graphical illustration of the proposed method. As can be observed, the images downloaded from the “GDXray” dataset have been improved by two distinct preprocessing stages. The first stage is to apply a CLAHE filter for contrast enhancement of the images. Then, some augmentations have been applied to increase the number of images (Hayati *et al.*, 2023; Xu *et al.*, 2023). This is done because the number of datasets for training a deep learning model is small.

The images are then trained by an RNN for the diagnosis task. As can be observed from the image, an EPOA has been applied to the network to improve the efficiency of the RNN. Finally, the network has been analyzed based on some different metrics, and its results have also been compared with state-of-the-art methods to show its superiority for using in the diagnosis task for welding applications.

4. Preprocessing

The preprocessing is an important stage in our work to prepare the data for the analysis and processing steps. This part includes two key components: contrast enhancement (based on CLAHE) and data augmentation. CLAHE is a powerful technique for enhancing the contrast of images, especially in cases where the contrast is low or the dynamic range is limited. In addition to contrast enhancement, the data augmentation technique is used to artificially increase the size of our data, which involves applying a series of transformations to the original data to produce new samples similar to the original data but with changes that help. In the following, the two methods are explained in detail.

4.1 Contrast enhancement

Contrast enhancement is an important stage in image processing that aims to improve the visibility of features in an image by adjusting the contrast between different regions. In this study, contrast-limited adaptive histogram equalization (CLAHE) has been used to enhance the contrast of X-ray welding images. The AHE divides the image into small regions called tiles and applies histogram equalization to each tile separately. CLAHE, on the other hand, limits the stretch of contrast to avoid excessive amplification of noise in the image. The CLAHE algorithm can be summarized by the following stages (Musa *et al.*, 2018):

- Dividing the original image into non-overlapping tiles, usually 8×8 (in this paper) pixels.
- Calculating the histogram of the tiles.
- Trimming the histogram to the maximum value, which is a user-defined parameter.

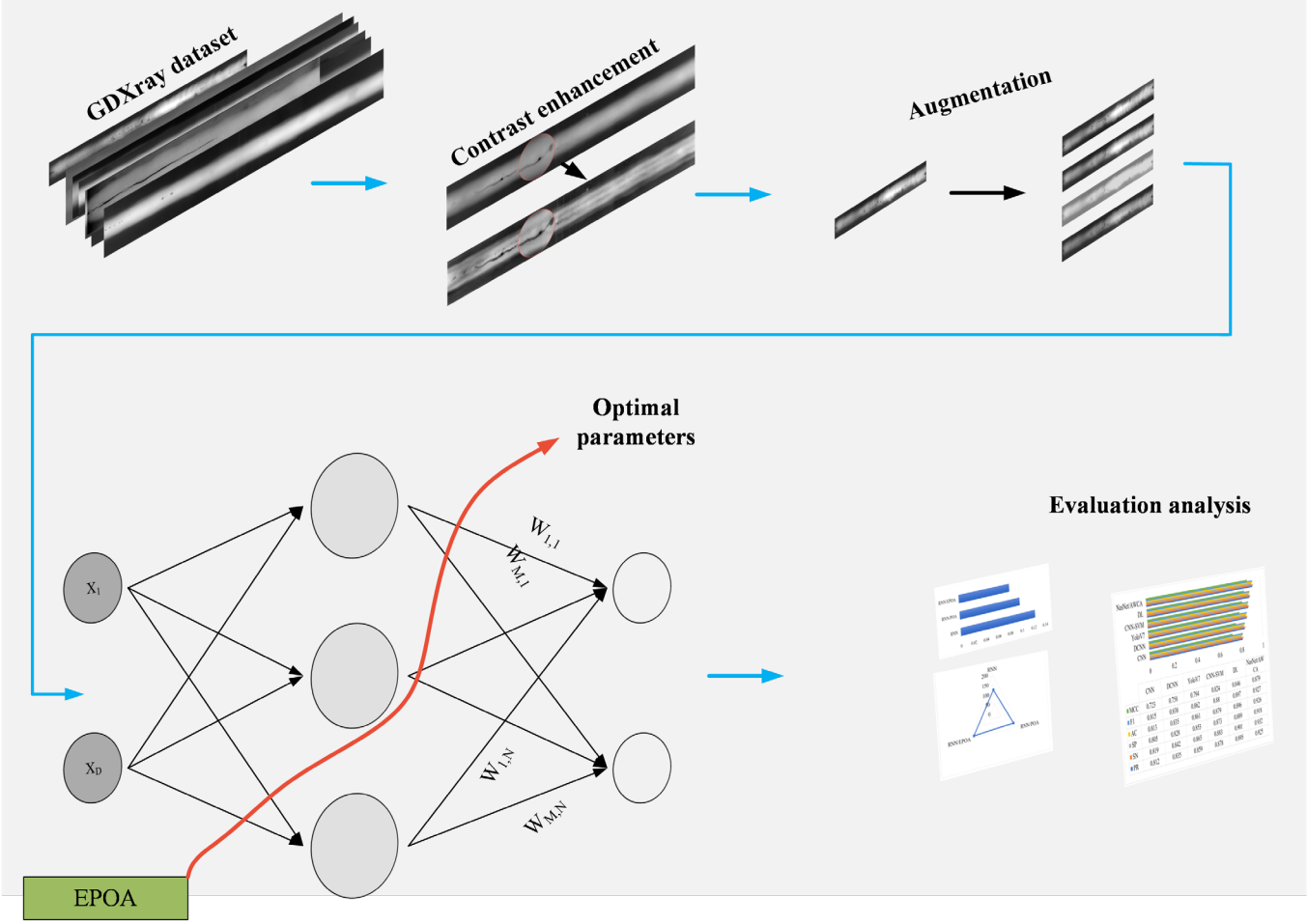

Fig. 2. The graphical illustration of the proposed method.

– Applying the histogram smoothing to the tiles based on the clipped histogram.
– Interpolating the results from the tiles to create a unified image

Fig. 3 shows an example of clarification of the effect of CLAHE on the welding image, with the top image showing the original image and the bottom image the improved image after applying CLAHE, along with the histograms of both images.

As can be observed from Fig. 3, the original image appears dark and lacks detail, with a narrow dynamic range, which makes it challenging to distinguish between different features, while the histogram shows a narrow peak with a low intensity value, indicating low contrast. Although the CLAHE-enhanced image shows a significant improvement in contrast and feature visibility, appearing brighter and more detailed, with a wider dynamic range, and a more uniform distribution of intensity values, with a higher peak value histogram, indicating contrast. Above, the CLAHE algorithm has effectively enhanced the contrast of the welding image, making it easier to distinguish between different features and increasing the contrast by stretching the intensity values. It improves the visibility of details and features and increases the dynamic range. This shows the effectiveness of CLAHE in enhancing the contrast and visibility of features in a welding image for image analysis and processing.

4.2 Augmentation

To enhance the size of the input dataset and strengthen the resilience of the model, various image augmentation techniques have been implemented on the original images. The augmentations included:

Flipping: Creating mirrored versions of the original images by flipping them horizontally and vertically.

Rotating: Generating new images by rotating the originals at angles of 180 degrees. Contrast Adjustment: Modifying the contrast levels of the images to produce variations in contrast (Xu *et al.*, 2023).

These augmentations were applied randomly to the original images, resulting in a more extensive and diverse dataset. The augmented images were subsequently utilized for training and testing our model, thereby enhancing its capacity to generalize new, unseen data. Fig. 4

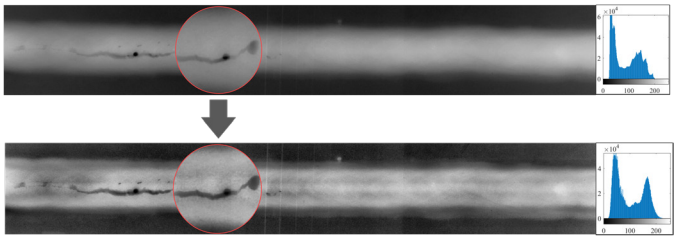

Fig. 3. One example of clarification of the effect of CLAHE on the welding image.

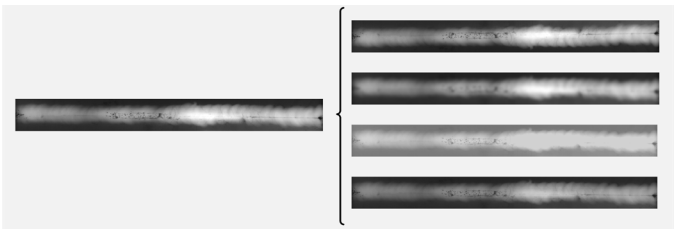

Fig. 4. Some examples of the augmentations performed on an original image.

Table 1.
Dataset statistics.

Category	Number of images	Series	Number of images per series
Welds	88	W0001	10
		W0002	10
		W0003	68

Table 2.
Dataset statistics after augmentation.

Category	Number of images	Series	Number of images per series
Welds	1760	W0001	200
		W0002	200
		W0003	1360

shows some examples of the augmentations performed on an original image.

Table 2 illustrates dataset statistics after augmentation.

Through these augmentation techniques, we successfully expanded our dataset and bolstered the robustness of our model, enabling improved performance on new, unseen data.

5. RNN

RNN has been considered an architecture of neural network that employs Rigdelet as a function of activation within the hidden layer. Rigdelet is the base of directional data description in domains with high dimensions and provides a better function in finding characteristics that are arranged based on particular orientations or directions. Rigdelet originates from the procedure of mathematical signals that are used for analyzing functions with the help of singularities of a hyperplane. The RNN could find and display directional information inside the data through merging Rigdelet in the hidden layer's function of activation (Wang *et al.*, 2024).

Rigdelet have been used for activation function in the RNN's hidden layer, because they can display functions with singularities of hyperplane. Such singularities are related to the occasions that functions represent unexpected changes or irregularities among specific hyperplanes. Rigdelet has been the best in demonstrating these functions, which makes it a great choice for the tasks that comprises finding hyperplane singularities.

The RNN and Rigdelet's cooperation could be beneficial in an exceptional way for implementing data with a high dimension, like vision of the computer recognizing, the patterns and procedure of image. The directional information, which Rigdelet is able to find, could help the network recognize and remove relevant features from the data, which in the end leads to improved action within tasks that need a directional consciousness of characteristics.

It is possible to achieve a more extensive comprehension and to be deeper to the subject that prepares particularized perceptions within the relation between Ridgelets in the neural network structure and emphasizes their benefits in displaying information of direction and operations with the singularities of hyperplanes. Actually, the results of the study include more data or modified versions of the RNN.

The conversion of Ridgelet is a mathematical procedure, which has been used to analyze and manage directional data. Its base is located in a function of neurons that $\psi : R \to R$ and is acceptable when it assembles the recommended situation. Soc, if it does not meet the recommended condition, it is not allowed.

$$K_{\psi} = \int \left(\frac{\hat{\psi}(\theta)^2}{|\theta|^d} \right) d\theta < \infty \tag{1}$$

here, the Fourier conversion of the ψ has been displayed by $\hat{\psi}(\theta)$.

The present situation guarantees that the function owns a limited energy and is square integrable. In fact, the transformation of Ridgelet uses the allowed function ψ in the input data during various directions for extracting the directional data characteristics. The neural network prepares the resulting converted data for the task of regression or performing the intended categorization.

Through considering the word ζ, a neuron area $\zeta = (a,u,b)$ could be obtained:

$$\mathrm{H} = \left(\zeta, a, b \in R, a > 0, u \in S^{D-1} \right), \tag{2}$$

$$u = 1 \tag{3}$$

Here, the placement of the Ridgelet function is displayed by b, the Ridgelet function's scale is represented by a, the orientation of the function of the Ridgelet is illustrated by u, and the S^D illustrates a sphere in area R^D.

When transformation, rotation, and the scaling process of the allowed functional neuron ψ is completed, a Ridgelet group could be extracted through utilizing the formula below:

$$\psi_{\zeta}(\theta) = \frac{1}{\sqrt{a}} \psi \left(\frac{\langle u, \theta \rangle - b}{a} \right) \tag{4}$$

where the Ridgelet direction is displayed by the variable θ. The Ridgelet, which is a result of the transformation, rotation, and scaling of the original function ψ, is illustrated by ψ_{ζ}.

The Ridgelets bank's use of the input data in various directions is a method applied by the Ridgelet conversion for extracting the data's directional characteristics.

Moreover, the transform of Ridgelet is an important device to estimate the singularities of hyperplane in a rapid way within a function group to be used for estimating function which are multivariate. Within present context, the function $[y \mid y = f(x) : R^n \to R^m]$ is divided into m computation $(R^n \to R)$, and the estimated multivariable function has been obtained employing the formula below:

$$\hat{y}_i = \sum_{j=1}^{N} c_{ij} \times \psi \left(\frac{\langle u_j, \theta \rangle - \beta_j}{a_j} \right) \tag{5}$$

$$u_j^{\,2} = 1 \tag{6}$$

$$\hat{y}_i = \left[\hat{y}_1, \hat{y}_2, \ldots, \hat{y}_m \right], \; i = 1, 2, \ldots, m \tag{7}$$

$$\theta, \; u_j \in R^D \tag{8}$$

here, the Ridgelet's superposition coefficient has been shown via c_{ij}.

An RNN that has one hidden layer could be improved by using the conversion of Ridgelet as the function of activation in the hidden layer. The transformation of Ridgelet has been applied to eliminate the input data's directional characteristics within different directions, after which it has been moved along the hidden layer. The Ridgelet coefficients achieved from the hidden layer are integrated in a linear manner to shape the RNN's output layer.

The structure of the RNN has been depicted in Fig. 5. First, the input data was converted by employing the transformation of the Ridgelet, which removes the data's directional characteristics. After that, the converted data was transported along the hidden layer where the transformation of Ridgelet was applied as the function of activation. Then, the coefficients of the Ridgelet produced by the hidden layer were integrated within the output layer for creating the network's final output.

The structure of the RNN has many benefits over traditional neural networks which are traditional. First of all, it is more effective in preparing directional data since it concentrates on the directional characteristics of the data, decreasing the neural network's calculation complexity. Then, it is less affected by the input direction, preparing it to be more resistant to changes within the data.

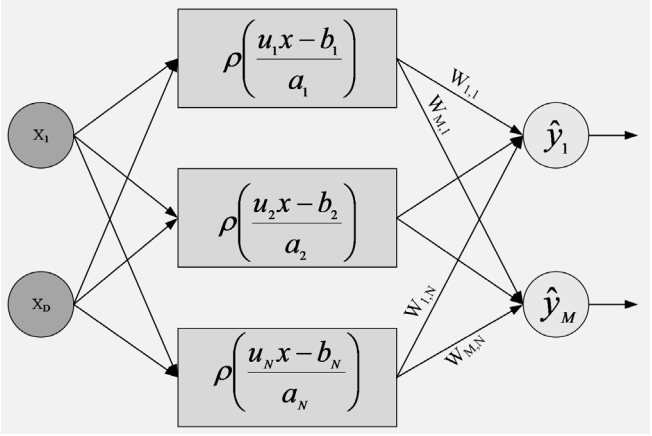

Fig. 5. The Ridgelet-NN's structure.

Lastly, it is displayed that traditional neural networks outperform in various applications, namely, seismic data analysis, medical image analysis, and remote sensing. The structure of the RNN is used in different areas within medical imaging, like X-ray. Within the analysis of medical images, RNN is utilized for segmenting, registering, classifying, and reconstructing the image. For instance, inside the recreation of the MRI image, the RNN is illustrated for decreasing the calculative complexity in comparison with the traditional neural network and enhancing the quality of the image.

A linear integration of the Ridgelets and weights (w_i) is use to enhance the Ridgelet-NN's estimation operation. The initial level in creating the Ridgelet-NN is to appropriately choose the network parameters. Such parameters have been explained below:

$$X = \left[w_1, w_2, \ldots, w_K,\ a_1, a_2, \ldots, a_K,\ b_1, b_2, \ldots, b_K,\ u_1, u_2, \ldots, u_K\right] \tag{9}$$

where the quantity of Ridgelets, employed in the network, is displayed via K, and the variables of the Ridgelet scalar are illustrated by a, b, and w, and the orientation is represented by u as follows:

$$\begin{aligned} u_1 &= \left[u_{11}, u_{12}, \ldots, u_{1m}\right],\ u_2 = \left[u_{21}, u_{22}, \ldots, u_{2m}\right], \ldots, \\ u_K &= \left[u_{K1}, u_{K2}, \ldots, u_{Km}\right] \end{aligned} \tag{10}$$

A linear integration of the Ridgelts and weights were applied by the Ridgelet-NN in order to estimate the input data. The RNN computes the coefficients of the Ridgelet within the hidden layer as a linear integration of the Ridgelets and the input data. The RNN's output layer is considered a linear integration of coefficients of the Ridgelet achieved from the hidden layer.

The scalar variables' choice (a, b, and w), the weights (w_i), and the vectors of Ridgelet orientation (u) are important for the RNN's operation. The existing parameters should be chosen in a proper way to guarantee the efficient extraction of the input data's directional characteristics and estimation of the intended output. The choice of the present parameters could be completed with the help of a trial-and-error procedure or algorithms' optimization and gradient descent. The network's k^{th} output neuron is computed employing this formula:

$$e_{kj} = y_{kj} - d_{kj} \tag{11}$$

where,

$$y_{kj} = f\left(\sum w_{lk} z_{kp} + w_{l0}\right) \tag{12}$$

here, $l = 1, 2, \ldots, m$.

For achieving a meticulous approximation of the issue, it is needed to decrease the cost function to its smallest quantity.

$$OF = \frac{1}{T}\sum_{j=1}^{L}\sum_{i=k}^{M} e_{kj}^2 \tag{13}$$

To obtain a precise estimation of the issue, the cost function needs to be reduced. This cost function is a sum of squared errors between the actual outputs and forecasted outputs in all of the instances of training, and it is divided by the training instances of total number (T). For minimizing the cost function, the parameters of the Ridgelet require to be chosen in an optimal way.

The primary goal of this search is to propose a novel change to an algorithm, which is metaheuristic, in order to obtain finer outcomes by choosing the parameters of the Ridgelet and reducing the cost function. The metaheuristic algorithm is a kind of optimizer that could be utilized to discover the optimum solution to a problem by exploring the solution space in an iterative way. The suggested change's purpose is to enhance the algorithm's effectiveness and efficiency within the optimum solution for the RNN.

6. EPOA

6.1 POA

In the beginning, the text explains the idea of algorithm's arrangement. Then, it outlines the essential processes for addressing optimization problems.

6.2 Inspiration

The Pufferfish is a Tetraodontiformes species and a member of the Tetraodontidae family. It is mainly found in marine and estuarine areas. Pufferfish have large spines just like porcupinefish, and they are usually small to medium-sized, growing up to 50 cm long (Al-Baik *et al.*, 2024). They are known for their beak-like teeth. They have four beak-like teeth. Such candidates have unique characteristics, such as a pelvis lacking pectoral fins and ribs. This design helps them inflate their bodies by taking in water through their mouth as a mechanism of defense.

Such individuals are famous for moving slowly, making them easy prey. However, they defend themselves by taking in a lot of water, turning into a big, spiky ball. This candidate has a sharp spine, which makes it difficult for hunters to eat, turning it from an easy target into a challenging one. While a predator notices this, it quickly retreats. The Pufferfish shows unique behaviors, including utilizing its defensive mechanism to turn into a big ball, which is spiky, and fighting with hunters. The determined algorithm (POA) offers a detailed demonstration of the way that individuals present natural manners in the following procedure.

6.3 Initialization

The current algorithm employs the population's abilities to find optimum solutions for optimizing problems inside the search space. It is worth mentioning that the current process has been iterative, and all of the individuals adjust their values of decision variables based on their location in the search space.

The POA consists of individuals represented as mathematical vectors, where all vector factors correspond to a decision variable. The population of the algorithm includes all members of POA, and their vectors are able to be represented in a mathematical way by employing the matrix shown in Eq. (3). The candidates' primary position is computed by Eq. (15).

$$Y = \begin{bmatrix} Y_1 \\ \vdots \\ Y_i \\ \vdots \\ Y_N \end{bmatrix}_{N\times m} = \begin{bmatrix} y_{1,1} & \cdots & y_{1,d} & \cdots & y_{1,m} \\ \vdots & \ddots & \vdots & \iddots & \vdots \\ y_{i,1} & \cdots & y_{i,d} & \cdots & y_{i,m} \\ \vdots & \iddots & \vdots & \ddots & \vdots \\ y_{N,1} & \cdots & y_{N,d} & \cdots & y_{N,m} \end{bmatrix}, \tag{14}$$

$$y_{i,d} = lb_d + e \times (ub_d - lb_d), \tag{15}$$

where, the variable Y demonstrates the matrix of the algorithm's population. The variable $y_{i,d}$ displays the dimension of d in the search

space. The variable m represents the number of decision variables. The variable Y_i shows the present algorithm's individual solution. The variable N specifies the number of candidates within the population. The d^{th} decision variable's lower bound is displayed through lb_d, and the higher bound of the d^{th} decision variable has been shown via b_d. The e factor illustrates a random quantity that is between 1 and 0.

In fact, the individuals are the potential solutions that are used for evaluating the problems' cost function. The cost function's evaluated values have been illustrated via a vector in the subsequent formula:

$$G = \begin{bmatrix} G_1 \\ \vdots \\ G_i \\ \vdots \\ G_N \end{bmatrix}_{N\times 1} = \begin{bmatrix} G(Y_1) \\ \vdots \\ G(Y_i) \\ \vdots \\ G(Y_N) \end{bmatrix}_{N\times 1} \tag{16}$$

where, the G variable shows the cost function's evaluated value. The assessed cost function is indicated by G_i, and it is on the basis of the i^{th} individual of the algorithm.

The cost function's evaluated value is a suitable requirement to estimate the amount of the individual solution recommended by the algorithm. The cost function's greatest evaluated value shows the optimum individual solution, but the least evaluated one illustrates the worst solution of the individual. All the iterations must enhance the candidate's situation within the search space, and the optimum individual solution must be improved in accordance with the cost function's recent evaluated values.

6.4 Mathematical model

The POA has improved the candidate's situation within the search space by replicating the natural manners of pufferfish and their hunters. Within the current process, the hunter attacks the pufferfish, and the pufferfish turns into a ball, employing its mechanism of defense that frightens the hunter. As a result, the individuals' situation is improved in two phases. The first phase involves a global search that includes the attack of the hunter's imitation. The next phase includes local search that mimics the individual's mechanism of defense.

6.4.1 Exploration

The procedure starts with simulating a hunter's attack to update the candidate's situation. Slow-moving individuals are not hard targets for predators because they make their positions easy to alter. During the predating process, the algorithm mimics the predator's moving to improve the individual's position in the search space. Through incorporating the hunters' technique, the algorithm improves its global search capabilities, leading to important modifications within the POV candidates' situations and the global search power enhancement.

The algorithm of POV treats each candidate as a predator. While discovering a fish in order to attack, it considers the other candidates' situation with a better action. The set of individuals for each of the populations is displayed below:

$$FQ_i = [Y_h : G_h < G_i, h \neq i]c, i = 1,2,\ldots,N\ k \in [1,2,\ldots,N] \tag{17}$$

Here, the situation of candidates' set for the i^{th} predator has been illustrated via FQ_i. The candidate with a high-cost function compared with the i^{th} hunter has been displayed via Y_h, and its cost function has been specified via G_h.

It is suggested that the predator selects a fish stochastically amid the fish in the FQ that are called chosen pufferfish (SP). By mimicking the predators' moving, a novel situation inside the search space is computed for POA candidates using Eq. (18). If the recent situation has enhanced the cost function, the new situation substitutes the former one employing the Eq. (19):

$$y_{i,j}^{Q1} = y_{i,j} + e_{i,j} \times (SP_{i,j} - K_{i,j} \times y_{i,j} \tag{18}$$

$$Y_i = \begin{cases} Y_i^{Q1}, G_i^{Q1} \leq G_i; \\ Y_i, else, \end{cases} \tag{19}$$

here, the randomly selected fish from the FQ_i set has been displayed via SP_i, and its dimension j has been shown via $SP_{i,j}$. Based on the recommended algorithm, the new situation of the predator i has been illustrated via Y^{Q1}, and its dimension j has been demonstrated via $y_{i,j}^{Q1}$. The cost function's value has been displayed via G_i^{Q1}. The random amounts have been shown via $e_{i,j}$. The constant $K_{i,j}$ has been equivalent to 2 or 1.

6.4.2 Exploitation

During the second phase, the candidate's position has been enhanced by stimulating the defensive mechanism of these fish. When they are threatened, they take in water in order to become a ball, deterring the predator. Through mimicking the predator's retreat movement, the algorithm can even detect small changes within the individual's position and increase its local search potential.

A new situation for a candidate could be calculated by simulating the predator's movement using Eq. (20). Consuming that the candidate's cost function has been improved, it will replace their prior situation employing Eq. (21). There have been many attempts to enhance the algorithm, leading to using the Eq. (21). An evaluation is arranged for cost function after finding a new situation for candidates. In the case that the cost function is greater than the prior one, the new situation is accepted, and in the case that it is not superior to the previous one, the candidate remains in their prior locations. Additionally, the update process for the individuals in the POA relies on the improvement of the cost function's value.

$$y_{i,j}^{Q2} = y_{i,j} + (1 - 2e_{i,j} \times \frac{ub_j - lb_j}{t}, \tag{20}$$

$$Y_j = \begin{cases} Y_i^{Q2}, G_i^{Q2} \leq G_j; \\ Y_i, \ else \ , \end{cases} \tag{21}$$

where, the predator's new situation has been shown via Y_i^{Q2} in accordance with the second phase of the algorithm, its dimension of j has been displayed via $y_{i,j}^{Q2}$. The amount of iteration has been demonstrated via t. The cost function's value has been represented through G_i^{Q2}. The $e_{i,j}$ variable is a random number ranging from 1 to 0.

6.5 Procedure of iteration

The algorithm's first iteration ends by improving the candidates' situation based on the local and global search. After that, the next stage of the algorithm begins, and the candidates' situation has been improved through using Eq. (17) to Eq. (21) until the final iteration. The optimum candidate's situation in each iteration has been improved and remains based on the evaluated cost function values. Eventually, the optimum candidate's situation suggests the solution.

6.6 EPOA

The POA has been considered a novel metaheuristic inspired by the pufferfish's natural manner and aimed at solving complex issues. In fact, its primary aim is to stimulate the pufferfish's defensive mechanism of inflating its body to scare the predators. The POA has been arranged to address the limitations of these optimization approaches, including computational costs, insufficient convergence, and low accuracy. The improved POA or IPOA introduces several improvements, including a harmony between local and global search, managing adaptive

parameters, and a new technique that all of them upgrade the capability of the algorithm's accuracy and effectiveness.

A major improvement is made through incorporating an adaptive weight element, which is nonlinear. This gets expanded in a finer solution space based on the candidate solutions' quality. This adjusting element is important because it avoids the population's early convergence and promotes the distinction, resulting in a better function. It must be mentioned that the improved equation of X might show fluctuations between the negative and positive values.

$$y_{i,j}^{Q1} = y_{i,j} + w_i \times \left(SP_{i,j} - K_{i,j} \times y_{i,j}\right) \tag{22}$$

The weight element of i^{th} value has been illustrated via w_i, and it has been calculated utilizing the following equation:

$$w_i = \frac{\bar{f} - f_i}{\bar{f} - \underline{f}}, i = 1,2,\ldots,N_P, \tag{23}$$

where the cost function's greatest value has been represented via $\bar{f}$, and its least value has been displayed via $\underline{f}$. The cost function of i has been demonstrated via f_i. Candidates with a lower quantity of cost functions are capable of exploring wider solution spaces through using a weighting element, while the ones with greater cost function values are limited to constrained solution spaces. The present approach assists in maintaining a harmony between the capacity of local and global search within the algorithm. Another improvement uses a chaotic map γ instead of random r through the subsequent formula:

$$y_{i,d} = lb_d + \gamma_t \times \left(ub_d - lb_d\right), \tag{24}$$

The current search employs Bernoulli shift map through using the subsequent equation:

$$\gamma_t^{new} = \begin{cases} \dfrac{\gamma_t}{1-\beta}, & 0 < \gamma_t \le 1-\beta \\ \dfrac{\gamma_t - (1-\beta)}{\beta}, & 1-\beta < \gamma_t < 1 \end{cases} \tag{25}$$

where, the quantity of iterations has been displayed via t, and $\beta = 0.4$. The Bernoulli shift map is capable of enhancing the algorithm's convergence.

This study uses the EPOA for computing the parameters of new fractional model to optimize the neural network for correction of writing. The present model has been represented in Fig. 6.

The main aim of this study is to enhance the architecture of the RNN by employing the EPOA to develop an effective system for detecting welding defects.

7. Results and Discussion

This section outlines the simulation outcomes of the proposed approach for detecting welding defects through the use of an RNN that has been optimized by the EPOA. Given the stochastic nature of metaheuristic algorithms, the results can differ with each execution. Consequently, each experiment was conducted 25 times, adhering to the parameter configurations.

Various other algorithms were employed for comparative analysis. To ensure a fair comparison, all algorithms were executed with a limit of 200 iterations (equating to 5,000 function evaluations). The programming was carried out in MATLAB R2019b 64-bit, and the computations were performed on a system equipped with an Intel Core i7 CPU running at 2.00GHz, 2.5GHz, with 16GB of RAM and a 64-bit operating system.

7.1 Algorithm validation of the EPOA

To validate the effectiveness of the EPOA, we performed a series of experiments. The algorithm was validated on a set of standard benchmark functions, consisting of around different functions extracted from the "CEC-BC-2017 test suite" that are continuously employed to assess the effectiveness of the algorithms. According to these functions, different varieties of the optimization problems have been evaluated. The results of the proposed EPOA are compared with five other metaheuristic algorithms, including Squirrel search algorithm (SSA), Billiard-based Optimization Algorithm (BOA), Black hole (BH), Locust Swarm Optimization (LS), and World Cup Optimization (WCO). Table 3 indicates the algorithm parameter values for the analyzed algorithms.

To confirm the robustness of the results, the comparative algorithm was run during 25 runs on each of the benchmark functions. Table 4 indicates the comparison results of the proposed EPOA with the other analyzed methods. This analysis is based on the mean value, the best value, and the standard deviation (StD) value of the objective function.

The results indicated in Table 4 highlight the superiority of the EPOA compared to the other methods examined. The EPOA consistently outperforms these algorithms regarding the best, mean, and standard deviation values of the objective function across all 12 benchmark functions. Notably, the EPOA secures the best results in 11 of the 12 functions, with the exception of F4, where it is surpassed by the SSA.

Furthermore, the EPOA demonstrates the lowest mean and standard deviation values in most functions, reflecting its capability to reliably converge towards the optimal solution. The results also indicate that

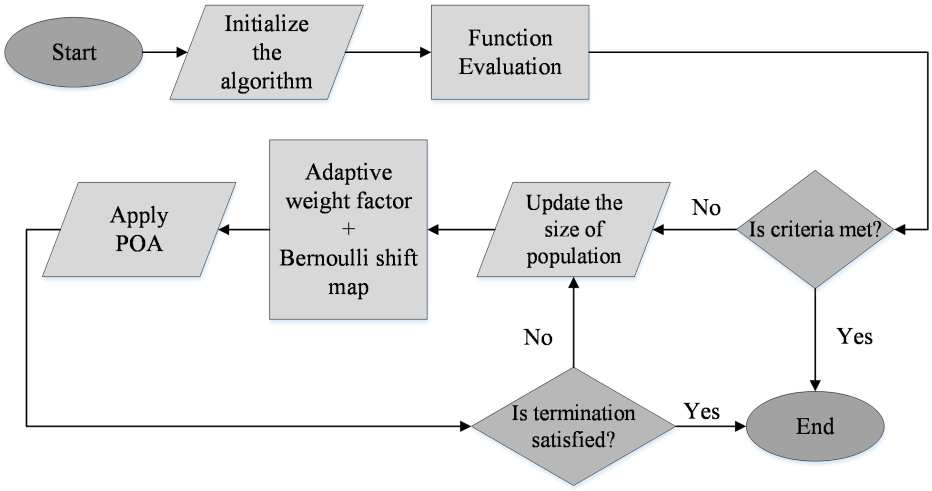

Fig. 6. The optimization of model on the basis of EPOA.

Table 3.
Algorithm parameter values for the analyzed algorithms.

Algorithm	Standard values	Reference
SSA	$N_{fs} = 4$, $G_c = 2$, $P_{dp} = 0.2$	(Jain *et al.*, 2019)
BOA	*No. of pockets* = 50, $w = 0.8$, $ES = 0.2$	(Kaveh *et al.*, 2020)
BH	$a = 0.5$, *Number of stars* = 200	(Hatamlou 2013)
LS	$F = 0.6$, $L = 1$, $g = 50$	(Cuevas *et al.*, 2020)
WCO	*Play* − *off* = 0.05, $ac = 0.5$	(Razmjooy *et al.*, 2016)
GA	Population size=100, Crossover rate=0.8, Mutation rate=0.01	(Alhijawi and Awajan 2024)
PSO	Swarm size=50,c1=2.0,c2=2.0,w=0.9	(Abualigah *et al.*, 2024)

the EPOA effectively addresses complex optimization challenges characterized by multiple local optima, such as F1, F2, and F3, where it significantly outshines the other algorithms. Additionally, the EPOA successfully attains optimal solutions in functions with multiple global optima, such as F12, where all algorithms reach the optimal solution. The EPOA's superiority can be attributed to its adaptive parameter adjustment and effective exploration of the search space, which enables it to evade local optima and converge to the global optimum. Its performance remains robust across various types of optimization problems, including both unimodal and multimodal functions, underscoring its versatility and efficacy as an optimization algorithm.

7.2 Preprocessing results

In this section, a comprehensive analysis was performed based on the RNN/EPOA architecture's performance prior to and following the

Table 4.
The comparison results of the proposed EPOA toward the other analyzed methods on the CEC-BC-2017 test suite.

Function	Index	SSA	BOA	BH	LS	WCO	GA	PSO	EPOA
F1	Best	2.392	67.745	0.889	1.686	48.349	1.154	1.287	0.952
	Mean	10.035	154.528	13.952	5.327	122.436	8.456	7.894	7.332
	StD	13.721	98.313	9.577	11.058	52.058	9.234	8.765	7.560
F2	Best	5.523	2.922	2.596	4.375	3.351	1.234	1.567	0.077
	Mean	84.484	47.579	40.168	48.031	34.909	45.678	42.345	0.377
	StD	27.894	37.281	25.850	17.568	36.084	28.987	26.789	0.630
F3	Best	1.352	25.954	18.170	1.199	20.359	0.123	0.156	0.009
	Mean	10.536	25.541	50.580	8.134	16.663	12.345	11.456	0.017
	StD	9.109	13.443	5.769	5.572	8.342	10.123	9.456	0.000
F4	Best	5.872	4.129	5.195	5.041	3.943	4.567	4.890	0.094
	Mean	6.907	6.033	4.230	3.111	3.563	5.678	5.234	0.118
	StD	1.809	1.400	0.539	0.900	0.755	1.234	1.123	0.072
F5	Best	0.157	2.722	3.934	0.133	2.205	0.056	0.078	0.000
	Mean	0.897	5.291	4.699	0.990	2.412	1.234	1.123	0.008
	StD	1.286	1.185	0.827	0.732	0.696	1.123	1.012	0.000
F6	Best	1.212	0.149	0.150	0.666	0.115	0.012	0.015	0.000
	Mean	1.094	0.989	0.561	0.801	0.592	0.567	0.512	0.000
	StD	1.716	1.523	1.215	1.098	1.089	1.123	1.056	0.000
F7	Best	0.487	0.723	1.273	0.401	0.358	0.567	0.589	0.651
	Mean	1.458	1.395	0.688	1.440	1.223	1.567	1.456	0.704
	StD	0.273	0.207	0.226	0.183	0.209	0.234	0.212	0.221
F8	Best	8.603	7.695	4.515	6.675	7.562	6.123	6.456	5.474
	Mean	21.869	15.700	14.493	14.896	11.700	16.789	15.678	10.033
	StD	4.453	4.352	2.554	2.150	3.215	3.456	3.123	3.411
F9	Best	0.145	6.521	8.126	0.107	5.794	0.023	0.034	0.000
	Mean	2.799	25.565	14.870	1.363	13.738	2.345	2.123	0.000
	StD	1.256	14.896	6.425	0.788	8.183	2.123	1.987	0.000
F10	Best	2.888	3.749	48.538	2.326	2.797	3.123	3.456	0.118
	Mean	10.923	8.230	154.679	7.430	7.544	12.345	11.456	2.242
	StD	7.027	5.260	15.932	6.825	6.055	10.123	9.876	2.608
F11	Best	0.120	0.084	0.058	0.066	0.050	0.012	0.015	0.000
	Mean	0.393	0.116	0.123	0.201	0.070	0.123	0.112	0.008
	StD	0.119	0.044	0.067	0.089	0.033	0.056	0.045	0.000
F12	Best	0.000	0.000	0.000	0.000	0.000	0.000	0.000	0.000
	Mean	0.000	0.000	0.000	0.000	0.000	0.000	0.000	0.000
	StD	0.000	0.000	0.000	0.000	0.000	0.000	0.000	0.000

Table 5.
The results of the welding defect detection, both pre- and post-preprocessing.

Model	PR	SN	SP	AC	F1	MCC
Before preprocessing	0.875	NA	0.801	0.894	NA	0.781
After preprocessing	0.895	0.925	0.845	0.915	0.909	0.835

implementation of the preprocessing technique. This technique was employed to resolve the issue of class imbalance present in the dataset. The objective of applying the preprocessing was to establish a more equitable representation of the welding data, thereby enhancing model performance and ensuring more accurate classification outcomes. The results and effectiveness of the RNN/EPOA architecture were assessed and compared in both scenarios to evaluate the influence of the preprocessing step on the model's overall performance. The results of the welding defect detection, both pre- and post-preprocessing, have been detailed in Table 5.

The findings illustrated in the results highlight the considerable influence of the preprocessing technique on the efficacy of the RNN/EPOA architecture in identifying welding defects. Before the implementation of preprocessing, the model recorded a precision of 0.875, a specificity of 0.801, and an accuracy of 0.894, while it was unable to report a sensitivity and F1-score due to class imbalance issues. Conversely, following the application of the preprocessing technique, there was a notable enhancement in the model's performance, achieving a PR of 0.895, SN of 0.925, SP of 0.845, AC of 0.915, F1-score of 0.909, and Matthews Correlation Coefficient (MCC) of 0.835. These outcomes suggest that the preprocessing technique successfully mitigated the class imbalance problem, resulting in a more equitable representation of the welding data and significantly improving the model's ability to detect welding defects.

7.3 Ablation analysis

To thoroughly assess the efficacy of our proposed methodology, an ablation analysis was performed to examine the contributions of each element within the design. Here, the following three variants were evaluated:

(1) Original RNN (RNN): This serves as the baseline model, lacking any optimization
(2) RNN with Original POA (RNN/POA): This variant merges the RNN with the original Pufferfish Optimization Algorithm.
(3) RNN with EPOA (RNN/EPOA): This represents our proposed approach, which integrates the RNN with the EPOA.

To assess the performance of each variant, a detailed array of metrics, including accuracy, precision, recall, F1-score, Mean Squared Error (MSE), and computational time, were employed. Accuracy was defined as the ratio of correctly identified welding defects, while precision represented the proportion of true positives relative to the total of true positives and false positives.

Recall was calculated as the ratio of true positives to the total of true positives and false negatives, and the F1-score was determined as the harmonic mean of precision and recall. Furthermore, we computed the Mean Squared Error (MSE) as the average of the squared differences between predicted and actual values, and we documented the computational time required for training and testing each model. This approach provided a comprehensive evaluation of each variant's performance concerning both classification accuracy and computational efficiency. Table 6 illustrates the classification performance of the ablation analysis.

Table 6.
Classification performance.

Model	PR	SN	SP	AC	F1	MCC
RNN	0.835	0.859	0.812	0.852	0.846	0.718
RNN/POA	0.862	0.903	0.822	0.885	0.882	0.775
RNN/EPOA	0.895	0.925	0.845	0.915	0.909	0.835

The results of the ablation analysis demonstrate the effectiveness of our proposed approach, with the RNN/EPOA variant achieving the best performance across all metrics, including precision, sensitivity, specificity, accuracy, F1-score, and MCC. Specifically, the RNN/EPOA variant achieves the highest precision, indicating its ability to correctly classify a higher proportion of true positives and reduce false positives, as well as the highest sensitivity, indicating its ability to detect a higher proportion of true positives and improve the model's ability to detect welding defects. Additionally, the RNN/EPOA variant achieves the highest specificity, accuracy, and F1-score, indicating its ability to correctly classify a higher proportion of true negatives, welding defects, and strike a good balance between precision and recall, respectively.

Furthermore, the RNN/EPOA variant achieves the highest MCC, indicating a strong correlation between the predicted and actual classes and demonstrating the effectiveness of the enhanced optimization algorithm in improving the model's ability to predict welding defects accurately.

7.4 Regression performance

In addition to analyzing the classification effectiveness of our proposed method, its regression performance is also examined by using the Mean Squared Error (MSE) metric. MSE quantifies the average squared deviation between the predicted values and the actual values of the welding defect severity. The results of the regression performance evaluation have been presented in Fig. 7.

The regression performance evaluation shows that our proposed RNN/EPOA shows superior performance in terms of MSE. This finding shows that the proposed EPOA significantly increases the model's ability to accurately predict the severity of welding defects.

In contrast, the original type of RNN shows the highest MSE, which reflects the largest mean squared deviation between the predicted and actual values. This result shows that RNN alone is insufficient to achieve accurate regression performance, and optimization is necessary to increase its effectiveness.

The variant RNN/POA shows a decrease in MSE compared to the original RNN, which indicates that the original POA positively contributes to the regression performance of the model. Nevertheless, the RNN/EPOA variant achieves an even lower MSE, which indicates that the advanced optimization algorithm is more adept at improving the regression capabilities of the model.

The increase in regression performance observed in the RNN/EPOA variant can be attributed to the superior ability of the advanced optimization algorithm to fine-tune the model parameters. This leads to more accurate prediction of weld defect severity, which is very important in industrial fields where accurate defect detection and classification are critical

7.5 Computational time

Computational time is a key factor in the creation of machine learning models, especially in industrial frameworks where prompt decision-making is important. In this research, we evaluated the computational time associated with our proposed method, RNN/EPOA, and compared it with the original RNN and RNN/POA variants. The findings from the computational time assessment have been displayed in Fig. 8.

The computational time evaluation results show that the RNN/EPOA variant requires the longest computational time, followed by the RNN/POA variant, and then the original RNN, which is expected to be increased due to the complexity added by the POA. The increased

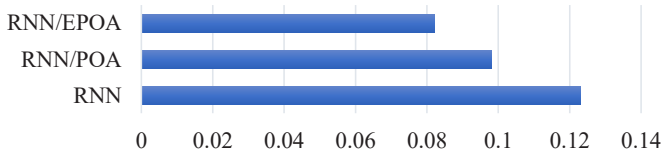

Fig. 7. The results of the regression MSE performance evaluation.

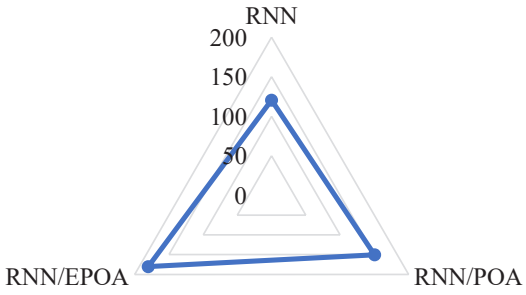

Fig. 8. The computational time assessment (seconds).

computational time of the RNN/EPOA type can be attributed to various factors, including optimization complexity, which is due to a more complex algorithm, model architecture, which is more complex with additional layers and connections, and more training data, which requires more calculations to optimize the model parameters. Despite the increased computational time, the RNN/EPOA variant achieves the best performance in terms of classification and regression accuracy, indicating that the improved optimization algorithm is effective in improving model performance, albeit at the cost of increased computational time, which represents a trade-off. There is a gap between model performance and computational efficiency

7.6 Comparative analysis

To comprehensively evaluate the performance of the current RNN/EPOA model, a 5-fold comparative analysis was performed with five existing models: Convolutional Neural Network (CNN) (Alhijawi and Awajan 2024), DCNN (Madhav *et al.*, 2023), YoloV7 (Block *et al.*, 2024), CNN-SVM (Yadav *et al.*, 2024), and deep learning (Vasan *et al.*, 2024). Comparison analysis was performed using the following criteria: precision, sensitivity, specificity, accuracy, F1 score, and MCC. The results of the 5-fold comparison analysis have been presented in Fig. 9.

The findings from the comparative analysis indicate that the RNN/EPOA model surpasses the current models regarding classification performance. The CNN and DCNN models exhibit lower values in precision, sensitivity, specificity, accuracy, F1-score, and MCC when compared to the RNN/EPOA model. Although the YoloV7 model performs slightly better than both CNN and DCNN, it still falls short of the performance demonstrated by the RNN/EPOA model. Furthermore, while the CNN-SVM and DL models show improved performance relative to CNN and DCNN, they do not reach the performance level of NasNet/AWCA.

7.7 Cross-validation analysis

To evaluate the reliability and robustness of the proposed RNN/EPOA model, we conducted a k-fold cross-validation analysis for the GDXray dataset. Cross-validation k is a very popular method to evaluate a model's performance by dividing a dataset into k subsets

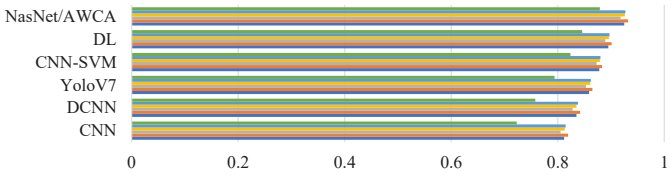

	CNN	DCNN	YoloV7	CNN-SVM	DL	NasNet/AWCA
MCC	0.723	0.758	0.794	0.824	0.846	0.879
F1	0.815	0.838	0.862	0.88	0.897	0.927
AC	0.813	0.835	0.861	0.879	0.896	0.926
SP	0.805	0.828	0.853	0.873	0.889	0.918
SN	0.819	0.842	0.865	0.883	0.901	0.932
PR	0.812	0.835	0.859	0.878	0.895	0.925

Fig. 9. The results of 5-fold comparison analysis.

Table 7.
Results of 10-fold cross-validation.

Fold	Precision (PR)	Sensitivity (SN)	Specificity (SP)	Accuracy (AC)	F1-Score (F1)	MCC
Fold 1	0.881	0.895	0.852	0.879	0.888	0.765
Fold 2	0.874	0.892	0.848	0.876	0.883	0.758
Fold 3	0.885	0.901	0.858	0.885	0.893	0.774
Fold 4	0.878	0.898	0.854	0.882	0.888	0.769
Fold 5	0.879	0.896	0.851	0.881	0.887	0.767
Fold 6	0.883	0.903	0.856	0.886	0.893	0.773
Fold 7	0.880	0.897	0.853	0.880	0.888	0.766
Fold 8	0.876	0.894	0.849	0.878	0.885	0.762
Fold 9	0.882	0.900	0.855	0.884	0.891	0.771
Fold 10	0.884	0.902	0.857	0.886	0.893	0.775
Average	0.880	0.898	0.853	0.882	0.889	0.768

(folds) and training the model on the k-1 folds and validating it on the kth fold. This is repeated k times, with each fold being the validation set one time. In this work, we developed a 10-fold cross-validation, allowing each image in the dataset to be used in both training and validation stages. Cross-validation analysis results show up in Table 7; in this table, we can see how many times our model was stable and generalizable.

Results of ten-fold cross-validation show that RNN/EPOA has performance and robustness invariant in different subsets of the data. Model performance, summarized in Table 7, demonstrates that the model behaves consistently across different configurations of the datasets, establishing its robustness and generalization ability. This negligible difference in performance across the folds illustrates that the model is not over-fitting towards certain parts of the dataset and has the capability to tackle varied patterns of welding defects. Additionally, the consistently high accuracy and F1-score corroborate that the model is able to minimize both false positives and false negatives, which is essential for defect detection applications. These results demonstrate the efficacy of the RNN/EPOA framework for practitioners and lend credence to its applicability for real-world welding defect detection tasks. However, more works are needed to stabilize the model by incorporating more regularization factors or increasing data sizes.

8. Conclusion

Welding is connecting the metal parts in general and steel parts using different methods. This can be done based on heat, pressure, or a combination of both. Welding defects production of healthy and defect-free welds, along with reducing costs, is one of the desired goals in the welding operation of metal structure joints. The main welding defects that cause the welding connection to break are among the things that every welder should be aware of. One of the most important reasons to be aware of these issues is the production of quality welds and the reduction of welding inspection time. The materials to be welded together (sheet or pipe) should be checked for weld surface defects. Because pipe welding defects are one of the most common defects. Image processing and machine learning as one useful Non-destructive techniques for this purpose. This study proposed a new method based on deep learning and a metaheuristic algorithm for the detection of welding defects. Here, a RNN was used as a classifier of the defects. The RNN efficiency was improved by optimizing its parameters to get optimal results. The optimization was performed by an EPOA. The proposed RNN/EPOA model was assessed using a benchmark dataset, called GDXray and its outcomes were compared with several leading techniques, including Convolutional Neural Network (CNN), DCNN, YoloV7, CNN-SVM, and Deep learning (DL) to demonstrate the superiority of the method. The results reveal that the proposed RNN/EPOA model can effectively identifying a range of welding defects. Future works will concentrate on enhancing the efficacy of the proposed detection system based on using different deep learning frameworks and optimization

techniques. A capable direction is to use transfer learning and domain adaptation methods to modify the system for this purpose. Moreover, incorporating additional NDT methods, such as ultrasonic testing and radiography, alongside the proposed system could yield a more holistic approach to defect detection. Also, the practical application in real-time or industrial settings may be hindered due to the high computational time, which can primarily be attributed to the sophisticated nature of EPOA. But this extra computational cost may be an impediment to implementing it in time-critical applications. Indeed, future studies can be also focus on improving model computational efficiency, either by simplifying the optimization algorithm applied, adapting it to the use of conventional methods such as parallelization or hardware revolution, preserving the performance achieved by the model. Sources of defects include more focused data, infinities; new methods of coding deeps. These would be the basis of making the higher-performance RNN/EPOA model more malleable and, more importantly, more useful in real-time applications where quick, accurate prediction of defect production is necessary. We will also focus on increasing the performance of the proposed detection system using other deep learning frameworks and optimization methods. Moreover, the study is not considering transferring learning to the proposed model, where the model, successfully trained on one dataset, can be used for a different dataset. Additive techniques such as transfer learning would enable the model to build on currently available networks and retrain on new datasets with less data loss. Meanwhile, domain adaption techniques could make the model adaptable to environmental or material-specific noise. Additionally, the addition of supplementary NDT techniques, including ultrasonic testing and radiography, harmonizing with the proposed system offered, would present a more comprehensive means of detecting defects covering wider industrial challenges.

CRediT authorship contribution statement

Tianmeng Ren: Conceptualization, Investigation, Methodology, Writing original draft, Conceptualization, Investigation, Visualization, Formal analysis.

Declaration of competing interest

The authors declare that they have no known competing financial interests or personal relationships that could have appeared to influence the work reported in this paper.

Data availability

The data can be freely accessible from the website: https://domingomery.ing.uc.cl/material/gdxray/.

Declaration of Generative AI and AI-assisted technologies in the writing process

The author confirms that there was no use of Artificial Intelligence (AI)-Assisted Technology for assisting in the writing or editing of the manuscript and no images were manipulated using AI.

Funding

Key scientific research project at the school level of Chengdu Aeronautic Polytechnic, "Research on a Chromium plated Connecting Rod Detection Platform Based on Machine Vision" (ZZX0623071).

References

Abualigah, L., Sheikhan, A., M. Ikotun, A., Zitar, R.A., Alsoud, A.R., Al-Shourbaji, I., Hussien, A.G., Jia, H., 2024. Particle swarm optimization algorithm: Review and applications. In: Metaheuristic Optimization Algorithms: Elsevier), pp. 1-14. https://doi.org/10.1016/b978-0-443-13925-3.00019-4

Al-Baik, O., Alomari, S., Alssayed, O., Gochhait, S., Leonova, I., Dutta, U., Malik, O.P., Montazeri, Z., Dehghani, M., 2024. Pufferfish optimization algorithm: A new bio-inspired metaheuristic algorithm for solving optimization problems. Biomimetics (Basel) 9, 65. https://doi.org/10.3390/biomimetics9020065

Alhijawi, B., Awajan, A., 2024. Genetic algorithms: Theory, genetic operators, solutions, and applications. Evol Intel 17, 1245-1256. https://doi.org/10.1007/s12065-023-00822-6

Block, S.B., Da Silva, R.D., Lazzaretti, A.E., Minetto, R., 2024. LoHi-WELD: A novel industrial dataset for weld defect detection and classification, a deep learning study, and future perspectives, IEEE Access 12, 77442-77453. http://doi.org/10.1109/ACCESS.2024.3407019

Mery, D., Riffo, V., Zscherpel, U., Mondragón, G., Lillo, I., Zuccar, I., ... & Carrasco, M. (2015). GDXray: The database of X-ray images for nondestructive testing. Journal of Nondestructive Evaluation, 34, 42. https://doi.org/10.1007/s10921-015-0315-7

Cuevas, E., Fausto, F., González, A., 2020. The locust swarm optimization algorithm. In: Intelligent Systems Reference Library, New Advancements in Swarm Algorithms: Operators and Applications (Cham: Springer International Publishing), pp. 139-159. https://doi.org/10.1007/978-3-030-16339-6_5

Cui, J., Zhang, B., Wang, X., Wu, J., Liu, J., Li, Y., Zhi, X., Zhang, W., Yu, X., 2024. Impact of annotation quality on model performance of welding defect detection using deep learning. Weld World 68, 855-865. https://doi.org/10.1007/s40194-024-01710-y

Hatamlou, A., 2013. Black hole: A new heuristic optimization approach for data clustering. Information Sciences 222, 175-184. https://doi.org/10.1016/j.ins.2012.08.023

Hayati, M., Muchtar, K., Roslidar, Maulina, N., Syamsuddin, I., Elwirehardja, G.N., Pardamean, B., 2023. Impact of CLAHE-based image enhancement for diabetic retinopathy classification through deep learning. Procedia Computer Science 216, 57-66. https://doi.org/10.1016/j.procs.2022.12.111

Jain, M., Singh, V., Rani, A., 2019. A novel nature-inspired algorithm for optimization: Squirrel search algorithm. Swarm and Evolutionary Computation 44, 148-175. https://doi.org/10.1016/j.swevo.2018.02.013

Kaveh, A., Khanzadi, M., Rastegar Moghaddam, M., 2020. Billiards-inspired optimization algorithm; a new meta-heuristic method. Structures 27, 1722-1739. https://doi.org/10.1016/j.istruc.2020.07.058

Li, L., Wang, P., Ren, J., Lü, Z., Li, X., Gao, H., Di, R.H., 2024. Synthetic data augmentation for high-resolution X-ray welding defect detection and classification based on a small number of real samples. Eng. Appl. Artif. Intell. 133, 108379. https://doi.org/10.1016/j.engappai.2024.108379

Madhav, M., Ambekar, S.S., Hudnurkar, M., 2023. Weld defect detection with convolutional neural network: An application of deep learning. Ann Oper Res. https://doi.org/10.1007/s10479-023-05405-3

Mery, D., Riffo, V., Zscherpel, U., Mondragón, G., Lillo, I., Zuccar, I., Lobel, H., Carrasco, M., 2015. GDXray: The database of X-ray images for nondestructive testing. J Nondestruct Eval 34, 42. https://doi.org/10.1007/s10921-015-0315-7

Musa, P., Rafi, F.A., Lamsani, M., 2018. A review: Contrast-limited adaptive histogram equalization (CLAHE) methods to help the application of face recognition. 2018 Third International Conference on Informatics and Computing (ICIC) Palembang, Indonesia, pp. 1-6. https://doi.org/10.1109/iac.2018.8780492

Mustafa, W.A., Yazid, H., Alquran, H., Al-Issa, Y., Junaini, S., 2024. Significant effect of image contrast enhancement on weld defect detection. PLoS One 19, e0306010. https://doi.org/10.1371/journal.pone.0306010

Palma-Ramírez, D., Ross-Veitía, B.D., Font-Ariosa, P., Espinel-Hernández, A., Sanchez-Roca, A., Carvajal-Fals, H., Nuñez-Alvarez, J.R., Hernández-Herrera, H., 2024. Deep convolutional neural network for weld defect classification in radiographic images. Heliyon 10, e30590. https://doi.org/10.1016/j.heliyon.2024.e30590

Razmjooy, N., Khalilpour, M., Ramezani, M., 2016. A new meta-heuristic optimization algorithm inspired by FIFA world cup competitions: Theory and its application in PID designing for AVR system. J Control Autom Electr Syst 27, 419-440. https://doi.org/10.1007/s40313-016-0242-6

Vasan, V., Sridharan, N.V., Balasundaram, R.J., Vaithiyanathan, S., 2024. Ensemble-based deep learning model for welding defect detection and classification. Eng. Appl. Artif. Intell. 136, 108961. https://doi.org/10.1016/j.engappai.2024.108961

Wang, F., Fu, S., Abza, F., 2024. Rigdelet neural network and improved partial reinforcement effect optimizer for music genre classification from sound spectrum images. Heliyon 10, e34067. https://doi.org/10.1016/j.heliyon.2024.e34067

Xu, M., Yoon, S., Fuentes, A., Park, D.S., 2023. A comprehensive survey of image augmentation techniques for deep learning. Pattern Recognition 137, 109347. https://doi.org/10.1016/j.patcog.2023.109347

Yadav, V., Banerjee, D., Sharma, N., Singh, V., 2024. Automated welding defect recognition through deep learning fusion: CNN and SVM integration. 2024 4th International Conference on Intelligent Technologies (CONIT) Bangalore, India, pp. 1-6. https://doi.org/10.1109/conit61985.2024.10627403

Zhang, R., Liu, D., Bai, Q., Fu, L., Hu, J., Song, J., 2024. Research on X-ray weld seam defect detection and size measurement method based on neural network self-optimization. Eng Appl Artif Intell 133, 108045. https://doi.org/10.1016/j.engappai.2024.108045